Motion of micro- and nano- particles interacting with a fluid interface

Stefano Villa, Giuseppe Boniello, Antonio Stocco, Maurizio Nobili

Motion of Micro- and Nano- Particles Interacting with a Fluid Interface

Stefano Villa[§,1], Giuseppe Boniello[§,2], Antonio Stocco[*3], Maurizio Nobili[4]

1. Università degli Studi di Milano, Dipartimento di Biotecnologie Mediche e Medicina Traslazionale, 20090 Segrate, Italy
2. Surface du Verre et Interfaces (SVI), UMR 125 CNRS/Saint-Gobain Recherche, 93303 Aubervilliers, France
3. Institut Charles Sadron (ICS), University of Strasbourg, CNRS, Strasbourg, France
4. Laboratoire Charles Coulomb (L2C), University of Montpellier, CNRS, Montpellier, France

§ These authors contributed equally to this work
*stocco@unistra.fr

Abstract

In this article, we review both theoretical models and experimental results on the motion of micro- and nano-particles that are close to a fluid interface or move in between two fluids.
Viscous drags together with dissipations due to fluctuations of the fluid interface and its physicochemical properties affect strongly the translational and rotational drags of colloidal particles, which are subjected to Brownian motion in thermal equilibrium. Even if many theoretical and experimental investigations have been carried out, additional scientific efforts in hydrodynamics, statistical physics, wetting and colloid science are still needed to explain unexpected experimental results and to measure particle motion in time and space scales, which are not accessible so far.

Introduction

Particles moving close to a fluid interface or straddling it are encountered in many research fields and applications ranging from Pickering emulsions, self-assembly, flotation, encapsulation, drug delivery, microrheology, microfluidics [1][2][3], and in material science [4]. Differently from solid boundaries, fluid interfaces coupled to a moving particle are the place of rich and complex dynamical phenomena. In the case of a particle moving close to a pure interface, hydrodynamics predicts that the particles viscous drag and its translational-rotational coupling both depend on the distance from the interface and on the viscosity ratio of the two fluid media [5]. In the case of a particle straddling an interface the key parameter for the particle drag is the particle contact angle which determine the partition between the two fluids with different viscosities [6]. Hydrodynamics can also be used to treat the situation when surface active species are present at the interface; a relatively high surface concentration of such species confers specific surface viscosities to the interface and changes the flow boundary conditions (BC) [7][8]. Even tiny quantity of such species may dramatically affect the BC as recently predicted [9]. In this latter case, the coupling between the surface flow induced by the particle motion and the Marangoni stress due to gradient in surface active species concentration may entail a surface incompressibility condition which greatly

affect the BC. It is expected that such condition enhances drastically the difference in the drag for a particle moving parallel or perpendicular to the interface.

From an experimental point of view, investigation of the behavior of a particle close to a fluid interface are relatively recent. Different techniques as optical tweezers [10], Dynamic Light Scattering [11] [12], and 3D video microscopy [13] has been used to measure the particle dynamics close to a pure interface while controlling and measuring its distance from the interface. In such cases, particles drags for both parallel and perpendicular motions with respect to the interface follows the prediction of hydrodynamic model with full slip boundary conditions. In the case of an interface with surface active species, recent experiments made in oscillatory conditions with a particle attached on a tip of an AFM and let be moved perpendicular to the interface show a more complex behavior. At high forcing frequency the particle drag follows the predictions of a full slip BC while at low frequency the drag is the one of no slip BC. Such a result has been successfully rationalized with the introduction of the surface incompressibility condition due to the Marangoni stress. Despite such experimental achievements a comprehensive study of both perpendicular and parallel drags in the case of an interface with a given concentration of active species is still lacking.

In the case of a particle straddling a fluid interface, experimental results follow the hydrodynamic prediction only at low particle contact angles, *i.e.* when the particle is immersed in the most viscous fluid [14] but they strongly deviate at large contact angle [15]. Such deviations have been attributed to the role of the triple line where the three phases (the two fluids and the solid) meet. Thermally activated triple line fluctuations may change its position on the particle surface and the contact angle giving rise to an extra dissipation further contributing to the particle drag. Finally, the theoretical and experimental achievements in this field have open the way to great improvement of surface microrheology techniques (i.e. the study of the interface properties via a particle probe) [16].

1. Motion of colloidal particles in the proximity of a fluid interface

1.1. Diffusion coefficients close to an interface

The motion of a particle immersed in a viscous fluid can be studied by solving the corresponding Navier-Stokes equation [17].

Here, we consider micro- and nano-particles with typical size a and velocity modulus v in the limit of a Stokes flow and at low Reynolds number ($Re = \frac{\rho_1 v a}{\eta_1} \ll 1$, where ρ_1 and η_1 are the density and the viscosity of the fluid). In this case, noting p the pressure, the Stokes equation, reads [17]:

$$\eta_1 \nabla^2 \vec{v} - \nabla p = 0 \ . \qquad (1)$$

If the colloidal particle translates at a velocity $\vec{v}$ and/or rotates at an angular velocity $\vec{\omega}$; it is subjected to translational and rotational viscous drags (respectively ζ^T and ζ^R).

For a spherical particle in an unbounded liquid, translation and rotation are decoupled. The relations between $\vec{v}$ (and $\vec{\omega}$) and the friction force $\vec{F}$ (and torque $\vec{\Omega}$) are obtained solving equation (1) for the associated flow fields, which lead to [17]:

$$\vec{F} = -\zeta^T \vec{v} \quad (2)$$

$$\vec{\Omega} = -\zeta^R \vec{\omega} \quad (3)$$

For a sphere of radius a in a homogeneous and unbounded liquid, with no-slip boundary conditions on its surface, the translational and rotational drag coefficients ζ_∞^T and ζ_∞^R write:

$$\zeta_\infty^T = 6\pi\eta_1 a \quad (4a)$$

$$\zeta_\infty^R = 8\pi\eta_1 a^3 \quad (4b)$$

In many real situations, however the fluid is confined by rigid walls and/or fluid interfaces. In a bounded fluid, spatial homogeneity and isotropy are broken and drag coefficients are function of the position of the particle and of the direction of the motion with respect to the boundaries. Moreover, such dependencies induce a coupling between the particle's translational and rotational dynamics.
For a particle moving at a velocity $\vec{v}$ close to a boundary the drag force writes:

$$\vec{F} = \zeta_\parallel^T v_\parallel \vec{e}_\parallel + \zeta_\perp^T v_\perp \vec{e}_\perp, \quad (5a)$$

where $\vec{e}_\parallel$ and $\vec{e}_\perp$ are unit vectors and the subscripts $\parallel$ and $\perp$ identify the direction parallel and perpendicular to the surface boundary respectively (figure 1). Similarly, for a particle rotating with an angular velocity $\vec{\omega}$ at a fixed position the hydrodynamics torque is given by:

$$\vec{\Omega} = \zeta_\parallel^R \omega_\parallel \vec{e}_\parallel + \zeta_\perp^R \omega_\perp \vec{e}_\perp, \quad (5b)$$

where $\omega_\parallel$ and $\omega_\perp$ refers to rotations around the axis respectively parallel and perpendicular to the normal to the interface (which is oriented along $\vec{z}$, see figure 1). $\zeta_\parallel^R$ and $\zeta_\perp^R$ therefore correspond to the spinning and rolling rotation drags respectively.
Note that translational and rotational drag coefficients are in principle tensors, but because of the symmetries of the considered system their contributions can be fully resumed introducing their components parallel and perpendicular to the interface. Moreover, drag coefficients $\zeta_{\parallel,\perp}^{T,R}$ are functions of the distance z_c between the particle center and the surface boundary (see figure 1).

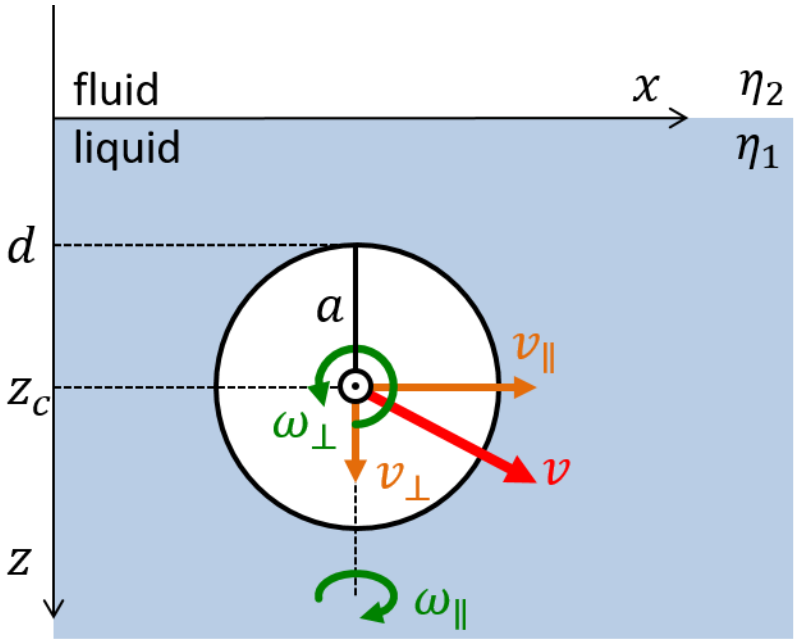

Figure 1: Sketch of the translational $\vec{v}$ and angular $\vec{\omega}$ velocities of a spherical particle of radius a in a bounded fluid. The fluid is bounded by a plane wall (fluid = liquid or gas) located at z =0 where z-axis is normal to the wall. z_c corresponds to the wall-particle center distance and $d = z_c - a$ is the minimal gap distance between the particle and the interface.

In general, $\zeta_\parallel^T$ and $\zeta_\perp^T$ (and similarly $\zeta_\parallel^R$ and $\zeta_\perp^R$) can be expressed as their bulk values corrected by non-dimensional factors $f_\parallel$ and $f_\perp$ (and similarly $g_\parallel$ and $g_\perp$ for the rotational drags).

Theories have been developed for the drags parallel and perpendicular to a plane for both no-slip (*i.e.* zero fluid velocity on the surface) and full-slip (*i.e.* zero shear stress on the surface) boundary conditions (BC). These conditions reflect the two limit cases of an interface between two fluid media. The full-slip BC (fs) refers to a particle moving in a bottom medium with a very high viscosity compared to the upper one, see figure 1. The no-slip BC (ns) applies to the reciprocal case: particle moving in a bottom medium with a very low viscosity compared to the upper one.

The theoretical predictions are typically functions of the scaled gap distance $h = d/a$, where d is the particle-interface gap distance. The translational drag coefficient for a particle moving perpendicular to the interface $\zeta_\perp^T$ has been obtained by Brenner [18], who determined the full series solution of the Navier-Stokes equations for both full-slip and no-slip BC.

In figure 2(a) the coefficients $f_\perp^{fs}$ (continuous line) and $f_\perp^{ns}$ (dashed line) are plotted as a function of h. For h >> 1, both $f_\perp^{fs}$ and $f_\perp^{ns}$ tend to 1, as expected far from the interface the drag coefficients result in the ones of the unbounded liquid. As h decreases, both $f_\perp$increase ($f_\perp^{ns}$ faster than $f_\perp^{fs}$) as the presence of a non-deformable boundary highly constraints the fluid flow accompanying the particle motion, and for $h < 0.1$ both $f_\perp$ diverges with an exponential trend.

The case of motion parallel to the boundary is more complex because of the coupling between translational and rotational degree of freedom.

The z dependency of the translational drag implies indeed that the viscous stress depend on the distance between the stress application point on the particle surface and the boundary, giving rise to a viscous torque on the particle. Accordingly, the application of a translational force on the sphere parallel to the interface generates also a rolling rotation of the latter along the axis parallel to the interface and perpendicular to the translational direction. Similarly the application of a rolling torque induces a translation parallel to the interface.

Such contributions are taken in consideration by introducing translational-rotational coupling terms t_{TR} and t_{RT} which complete equation (2) and (3) for the considered motions:

$$F_{\parallel} = -6\pi\eta_1 a\left(v_{\parallel} f_{\parallel}' - a\omega_{\perp} t_{TR}\right) \quad (6)$$

$$\Omega_{\perp} = -8\pi\eta_1 a^3 (a\omega_{\perp} g_{\perp}' - v_{\parallel} t_{RT}) \quad (7)$$

Where $f_{\parallel}'$ and $g_{\perp}'$ indicates translational and rotational non-dimensional drag coefficients for a particle forced to translate without rotation and forced to rotate without translation respectively.

Because of the symmetries of the system, the terms coupling rotation and translation along the other axes are all equal to zero.

In the case of a freely diffusing particle, the common thermal origin of both translation force and rotational torque makes possible to synthetize equations (6) and (7) with the expressions (5a) and (5b), where $f_{\parallel}$ is given by the cooperation of pure translational drag ($f_{\parallel}'$) and roto-translation coupling (t_{TR}) while $g_{\perp}$ rises from the contributions of pure rotational drag ($g_{\perp}'$) and roto-translational coupling (t_{RT}).

In 1967 Goldman, Cox and Brenner (GCB) [19] found numerical solutions of Stokes equation for the translational and rotational drag coefficients of a sphere moving parallel to an interface with no-slip BC. They also derived two asymptotic solutions respectively for a particle-interface gap distance much smaller than particle radius ($h \ll 1$), using lubrication-theory, and for the opposite limit ($h \gg 1$) using the method of reflections.

Nguyen and Evans (NE) [20] more recently found the corresponding numerical solutions for completely slip BC. They also developed analytical approximated expressions of both their and GCB's numerical solutions for the parallel translation drag in the whole range of separating distances, see figure 2b.

In figure 2(b), the analytical approximated values of $f_{\parallel}^{fs}$ (solid line) and $f_{\parallel}^{ns}$ (dashed line) are plotted versus h. As for the perpendicular drags, parallel drags approach the bulk value when h >> 1. For the no-slip BC, the parallel drag increases when the particle approaches to the interface. The drag is however much lower than the corresponding perpendicular one taken at the same distance from the interface and no exponential trend is found when h < 0.1. On the other side, for full-slip BC the parallel drag takes a finite value lower than the bulk one as the particle approaches the interface ($f_{\parallel}^{fs}$= 0.734 for h = 0). The decrease of the parallel drag at small distances in this case is due to the negligible viscosity (e.g. air) of the top fluid which not carry the particle.

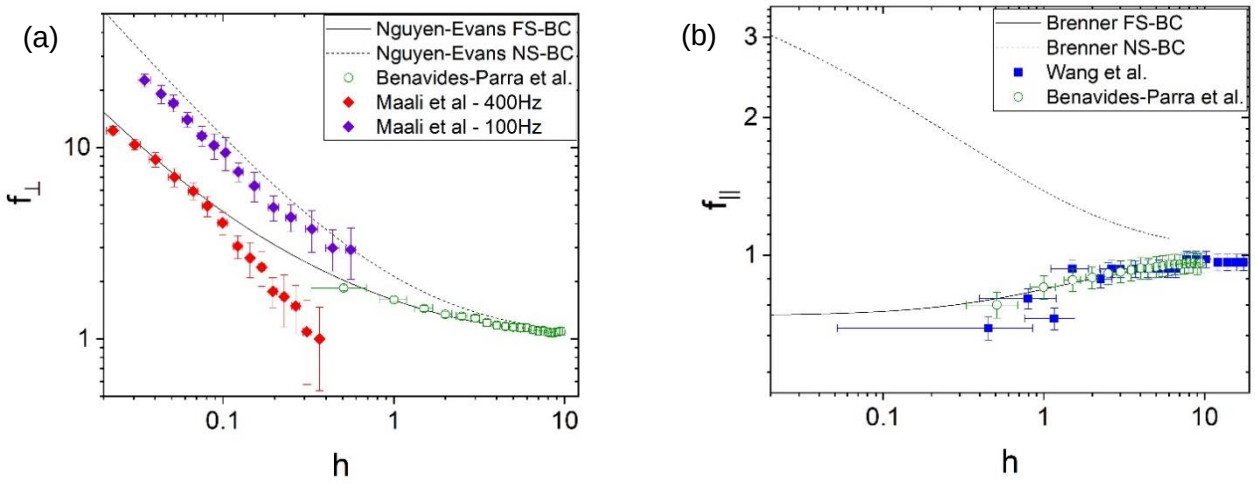

Figure 2: Non-dimensional perpendicular $f_\perp$ (a) and parallel $f_\parallel$ (b) drag coefficients versus $h = d/a$ (the ratio between the gap distance and the radius) in the case of full slip (continuous line) and no-slip (dashed line) boundary conditions accordingly to the models of Brenner and NE for $f_\parallel$ and $f_\perp$[19] [20]. Experimental data close to air-water interfaces are also reported: Benavides-Parra *et al.* [13] (green circles, (a) and (b)) and Maali *et al.* [9] for a sphere forced to oscillate at 100 Hz (purple diamonds, (a) and 400 Hz (red diamonds, (a)) in the direction perpendicular to the interface, Wang *et al.* [10] (blue squares, (b)). Wang *et al.* [10] and Benavides-Parra *et al.* [13] data are reported with their effective experimental incertitude, while the error bars reported for Maali *et al.* [9] are obtained averaging over several experimental points at different values of h.

The drags represented in figure 2 describe two limit cases: full slip BC account for a particle moving in a high viscous fluid close to the interface with a low viscous fluid (corresponding to the case of particle in water close to the interface with air), while no-slip BC corresponds to a particle moving in a low viscous fluid close to an interface with an high viscous fluid (corresponding to the case of a particle in water close to an interface with an highly viscous oil). In the general case, particle drag coefficients depend on the viscosity ratio $\lambda = \eta_1/\eta_2$. L. G. Leal elaborated both analytical approximated formulae [21] and numerical calculations [22] for a generic value of λ. The analytical model is made in the point-force approximation thus holding for h >>1. As a result, the found solution differs largely from the exact solution when $h < 1$ and misses the divergence when $h \to 0$.

The calculation of the spinning rotation drag coefficient $g_\perp$ is also reported in the works of Lee *et al.* [21] [22], where also the complete roto-translation dynamics is discussed for both slip and no-slip interfaces.

In particular, a change in the sign of the roto-translational coupling from rolling to anti-rolling is predicted when the normalized translational drag on the particle goes from $f_\parallel > 1$ to $f_\parallel < 1$. Such a change in particle drag occurs when the upper fluid has a viscosity larger than the bottom fluid containing the particle [22]. As a consequence for a given λ one can find a distance h_0 where such coupling is exactly zero. For distances shorter than h_0 the particle rolls over the interface like a wheel on the ground, while for $h > h_0$ for the same particle subject to the same translational force reverse the sign of its rotation.

1.2. The key importance of boundary conditions

Beyond the two BCs treated in the previous section, fluid interfaces can also support other boundary conditions. They applies when molecular or larger species (surfactants, contaminants, ions,...) different from the ones of the two bulk fluids are present at the interface.

At a gas-liquid interface such species affect particle dynamics in two ways. First, they can produce Marangoni flows that resist to the interfacial flux originated from the particle motion, and second, they give rise to a surface viscosity.

In 1913 Boussinesq [23] introduced the concept of surface viscosity, while in 1960 Scriven [24] discriminated between the dilatational (η_d) and the shear (η_s) surface viscosities.

Interfacial rheology methods have been designed to measure surface viscosities in the limit of large surface concentrations in order to obtain Boussinesq numbers: $n_d = \eta_d/a\eta_1$ and $n_s = \eta_s/a\eta_1 > 1$ (with a negligible bulk contribution to rheology). Danov *et al.* [5] provided numerical results for the translational and rotational drag on a spherical particle as a function of h, λ, η_d and η_s, showing that at small distances the surface viscosity is responsible of a substantial increase of both translational and rotational drags. Important differences from the bare interface case appear when the Boussinesq numbers are larger than 1. A discussion on the effect of surface viscosity on rotational drag can be also found in the work of Davis and O'Neill [25].

The opposite limit of low surface concentrations is governed by Marangoni stress, whose effect on the boundary conditions has been taken into consideration only recently [26]. Particle motion induces an interfacial flow which perturbs the local concentration of surface active species generating a concentration gradient. This surface concentration gradient is associated to a Marangoni stress, which in turn induces an opposite molecular flow, resulting in a condition of incompressibility for the interfacial flow ($\nabla_s \cdot u_s = 0$, where u_s is the fluid velocity at the interface).

For a spherical particle in water oscillating in the direction perpendicular to a gas-liquid interface at frequency ν, a model has been proposed in 2017 by Maali *et al.* [9]. The model considers an ideal gas behavior of the surface active species, whose concentration follows an advection-diffusion equation. The velocity field in the liquid between the gas and the particle is treated in standard lubrication theory. Accordingly to this model, in the quasi-static limit when the time scale of particle motion is much larger than the typical relaxation time of the concentration gradient of surface active species, the fluid cannot flow any more on the interface because of surface incompressibility.

The contribution to the particle drag of such effect depends on the ratio between the imposed frequency ν and a characteristic frequency ν_0 given by:

$$\nu_0 = \frac{c_0 k_B T}{8\eta_1 a}, \tag{8}$$

where c_0 is the 2D concentration of the surface active species at the interface. When $\nu \gg \nu_0$ the particle drag is the same as the one for a pure gas-liquid interface, i.e. full slip BC. Quite strikingly, in the opposite limit ($\nu \ll \nu_0$) the particle drag is the one predicted for no-slip BC.

The interfacial flow resulting from the combined effect of a Marangoni stress and the particle motion has been addressed more in detailed by Bickel *et al.* [7]. In this work, a limiting radius on the interface is defined. Such radius divides an inner region where surface active species are advected by the interfacial flow, and an outer one where such species accumulate building up the Marangoni stress which prevents further radial flow. The value of the delimiting radius is highly sensitive to the surface species concentration, and thus to the surface tension. As suggested by the author, the measurement of the delimiting radius can therefore in principle be used to obtain the surface tension with a resolution improved of orders of magnitude compared to standard techniques [7].

Particle parallel drag is also affected by the presence of low concentration of surface active species. Theoretical treatment of this case is more complex because of the coupling with the particle rotation and the lack of polar symmetry for the surface flow. Bławzdziewicz *et al.* [26] have numerically computed the parallel drag in the quasi-static limit. From their analysis it results that $f_{\parallel}$ is less affected than $f_{\perp}$ by surface incompressibility: parallel drag is lower than in the bulk and about 14% higher than the one of the compressible case as the surface incompressibility condition add supplementary constraint on the flow.

Measurements of particle viscous drags close to boundaries were first obtained in the case of solid walls. Experimental evidences of enhanced drag coefficients were already known in 1961 [27], but the poor control and precision on the particle-boundary distance prevented any quantitative measurements until 2007 [28]. Then, a number of experiments has been made with different techniques like video microscopy [28], dynamic light scattering [29], total internal reflection microscopy [30] and oscillating optical tweezers [31]. These experimental investigations validated Brenner and GCB models for no-slip BC [18] [19].

Experimental investigations of the liquid-gas interfaces are more recent. The h-dependency of the parallel drag was first measured by Wang et al- in 2009 [10]. They studied the motion of isolated silica particles in water confined by an optical trap. The optical trap allowed the control of the distance from either an air-water or an oil-water interface. They tracked the motion of the particle parallel to the boundary after trap release by bright field microscopy and verified that the diffusivity was enhanced close to the air-water interface and reduced close to the oil-water one. They follow the particle motion on planes parallel to the interface located at different distances from it. Each plane was spaced by 1 µm (about 1/5 of the particle diameter). To define an absolute particle-interface distance, they consider as the zero gap distance the location at which interfacial forces pull the particle out of the trap. This procedure limits the resolution of the particle-interface distance to 100 nm, corresponding to the range where the interfacial forces become comparable to the strength of the optical trap. Consequently they were not able to measure particle drag at very short distances (h < 0.5) where it more dramatically deviates from the bulk value.

In 2014 Watarai *et al.* [11] first measured the drag perpendicular to an air-water interface using a dynamic light scattering (DLS) technique based on a Michelson interferometer coupled with a low-coherence light source. In low-coherence DLS, the collected scattering volume is relatively small allowing the measurement of its distance from the boundary. They access in this way to the measurement of the diffusion coefficient of monodisperse submicrometric particles as a function of the position [29] with a spatial resolution of the order of the micrometer. As in the work of Wang *et al.*[10], the short range particle-interface distances where drag most deviates from its bulk value were not explored.

The complete 3D trajectory of a colloidal spherical particle was first measured only in 2016 by Benavides-Parra *et al.* [13]. They used 3D digital video microscopy to measure both parallel and perpendicular drag of a spherical particle of 0.5 µm radius and for particle-interface distances $d \leq 10$ µm. Measurements were made with a resolution in the particle-interface distance of 0.1 µm, in the same range as both Wang *et al.* [10] and Watarai *et al.* [11]. Moreover, Benavides-Parra *et al.* verified that in the case of a namely pure air-water interface is superfluous to consider the air viscosity, as they found the same agreement with data either considering it ($\lambda = 80$) or neglecting it [13]. Data collected near air-water interfaces can thus be rationalized neglecting the effect of air viscosity and considering theoretical prediction for full-slip boundary conditions at the interface. Note that effects of surface compressibility were not taken into account in these three works.

Recently, high resolution measurements of the particle perpendicular drag close to an air-water interface have been carried out by Maali *et al.* [9]. The perpendicular drag was measured using a spherical particle attached on an AFM tip and forced to oscillate at a given frequency in the direction normal to the interface. Differently from previous experiments, the large particle size (about 50 µm) allowed to access at very small values of h down to 0.02, see figure 2.

The measured drag depends on the oscillation frequency. At the relatively high frequency it follows the predicted value for slip BC as expected. At low frequency (100Hz), instead, it increases reaching the value corresponding to no-slip BC. Such experimental results are in good agreement with the model developed by the same authors of surface flow incompressibility due to gradients of surface active species and the related Marangoni stress.

This result highlights how sensitive is the drag at very small particle-interface gap distances to the presence of minimal concentrations of active molecules at the interface as the presence of such molecule can drastically change the flow BC.

1.3. Towards contactless surface microrheology

The mentioned sensibility of submerged particle motion to surface viscosity encouraged in recent years the development of contactless surface active micro-rheology. This method relies on the measurement of the force felt by a micrometric particle moving in the plane parallel to the interface at a given particle-interface distance using an optical trap. Such methodology overcomes the ambiguity of interface macrorheology while keeping the analysis simpler than in contact microrhelogy, as it avoids the issue related to the understanding of the not trivial interaction between the interface and the particle probe [32] [33]. Some articles have been dedicated to analyze this opportunity [34,35], which allows the study of the rheological properties even of phases with very low viscosity ($\approx 10^{-9}$ N.s.m^{-1}). This new method together with the possibility to probe extremely low surfactant concentrations through the measurement of surface compressibility is very promising for a non-invasive and extremely accurate investigation of air-water interface.

Note that not only the translational drag is very sensitive to surface shear viscosity effects but also the rolling rotational drag (rotation along an axis parallel to the boundary). In the high Boussinesq number limit, the rolling rotation of a spherical particle close to a gas-liquid interface should coincide with the rolling motion of a sphere close to a solid wall [6]. In the opposite limit of small surface shear viscosities, instead, the particle rotation may even switch sign as opposite to the one of a wheel on a solid boundary.

1.4. Non hydrodynamic contributions to the drag

In most real situations, colloid motion is not only determined by hydrodynamics. Real colloidal systems are often characterized by the double layers interactions due to electrostatics. An electrostatic double layer is also present at the water-fluid interface, which exhibits a negative surface potential [36].

Whenever a charged phase (a solid particle, or a gas/liquid phase) is in contact with a liquid electrolytic phase, a double-layer of ions and counterions builds up around the charged boundary. Hence, if one charged phases moves relatively to another phase, the flow deforms the double-layer. From the coupling of hydrodynamics and electric forces a number of phenomena arises, grouped under the name of electrokinetic effects.

The measured quantity in electrokinetic experiments is usually the Zeta potential. It is defined as an electric potential evaluated on an imaginary surface (i.e. surface of shear) around a charged object which encloses a volume where the fluid is always stationary. Zeta potential is directly related to the mobility of the charge particle and includes the effects of the surface potential and of the charges contained inside the surface of shear.

From a theoretical point of view, electrokinetic effects are studied coupling the Poisson equation for the electric potential with a convective-diffusion equation determining the distribution of ionic charges in the liquid. Since the solution of this set of equations is a formidable task even in the simplest geometries, usually approximations are studied in the limit of low Péclet number, corresponding to diffusion dominated dynamics with respect to convection.

Here, we report two effects which can be relevant for the dynamics of a micrometric or nanometric particle moving near a plane boundary [37]: the electroviscous drag and the electrokinetic lift.

The first one arise from the distortion of the double-layer due to the flux. This modification, in turn, alters the local hydrodynamic flow around the particle leading to an increment of energy dissipation. This energy dissipation occurs even in the case of a stationary motion, as the ions of the double-layer are dragged away and other ions are attracted by the particle, generating a new flux, which is the responsible of the additional dissipation.

In 1984 Oshima *et al.* [38] derived an expression for the electroviscous drag for a charged spherical particle translating in a bulk solution. In 2006, Tabatabei *et al.* [39] found an expression for the electroviscous force acting on a spherical particle moving parallel and close to a plane with no-slip boundary conditions and with a finite Zeta potential. They found that the component of the electroviscous drag parallel to the interface increases as a^2/d^2 approaching to the boundary. Accordingly, at very small distances the electroviscous drag increases more rapidly than the hydrodynamic one.

Beyond the effect on the drag coefficients, electrokinetics effects gives rise to a lift force perpendicular to the surface, first observed in 1987 by Prieve and Bike [40].

In 1997, Cox [41] elaborated a general theory coherent to previous experimental observations. According to the theory, the dominant contribution to the electrokinetic lift force comes from the hydrodynamic stress arising from the electroviscous flow along the surface of the particle. The expression of the lift force on a cylindrical particle has been used by Warszynski [42] to estimate such force on different geometries. In the case of a solution with two ionic species, the resulting expression for the lift force on a spherical particle moving parallel to a no-slip boundary varies linearly with h, $f_{\parallel}$ and $g_{\perp}$.

1.5. Perspectives

Different BC at a fluid interface from the usual slip BC are not anecdotal as many examples have emerged in these last years [43][44][45]. In the future, a deeper understanding of BC at water-fluid interface will be important for the understanding of a variety of phenomena like micro- and nano-particle adsorption dynamics and artificial/biological (e.g. bacteria) microswimmer motion in the vicinity of a water-fluid interface.

The spatial resolutions of the experimental works in literature was sufficient to verify theories of Brenner, GCB and NE but were not able to sense subtler effects recently predicted like the one of surface incompressibility on the particle drag parallel to the interface. To the best of our knowledge, there are no experimental observations reporting the effect of surface incompressibility on the parallel particle drag and on the rotational one [26]. Experimental investigations on contributions of surface incompressibility to translational and rotational motion of colloidal particles in the proximity of a fluid interface is therefore highly demanded.

Finally, the role of electrokinetic effects on the particle motion close to a fluid interface remains largely unexplored, as up to now, experiments were performed in conditions tending to minimize electrokinetic contributions, using for instance significant amount of salts in the liquid phase [13].

2. Motion of partially wetted colloidal particles at a fluid interface

2.1.Translational and rotational drags as a function of the particle immersion or contact angle

Micro- and nano-particle motion could also occur in between two immiscible fluids when straddling the interface between them, see figure 3.

A solid colloidal particle at a fluid interface in a partial wetting state is usually trapped in a surface energy well [46][47]. The order of magnitude of the energy well can be roughly estimated by the surface energy of the portion of the fluid interface occupied by the particle: $E = \sigma\pi a^2$(for a spherical particle with a 90° wetting contact angle θ, see figure 3), where σ is the fluid interfacial tension and a the particle radius. This energy is of the order of 10^6 - 10^7 k_BT for ideal micrometric particles, which is very high if compared to thermal agitation (k_BT). Hence, vertical particle motion should be suppressed and micrometric particle adsorption at the interface can be considered as irreversible. Different is the case for nanometric particles, where a potential well of tens of k_BT may allow vertical movements.

Note that even for microparticles a slow vertical motion at the interface can be observed during relaxation toward the equilibrium vertical position, as reported by Kaz *et al*. [48]. Such a motion is due to contact line dynamics, as we will describe in 2.2.

The vertical equilibrium position of a particle at the fluid interface is given by the balance of the three interfacial tensions involved in the system: liquid-fluid, solid-liquid, solid-fluid (figure 3). This force balance, written as a function of the particle position with respect to the interface (or contact angle), gives the well-known Young's relation. While the vertical particle motion is strongly confined or even suppressed, on the contrary the particle can freely move parallel to the interface. Knowing the translational Stokes friction in the bulk, $\zeta_\infty^T = 6\pi\eta_1 a$, one might

expect that the parallel viscous drag experienced by a particle partially immersed in (or partially wetted by) two fluids is an average between the drags of the two fluids, weighted by the particle immersion depth in each phases. For this reason, the translational drag parallel to the interface is expected to be dependent on the particle contact angle, $\theta = \mathrm{acos}(z_c/a)$, see figure 3. For some particular cases, when η_1 >> η_2 (i.e. water-air, oil-air, highly viscous oil-water), the contribution of the less viscous phase can be neglected in the theoretical models describing the viscous translational drag of a particle straddling a bare interface, which depends only on θ and η_1.

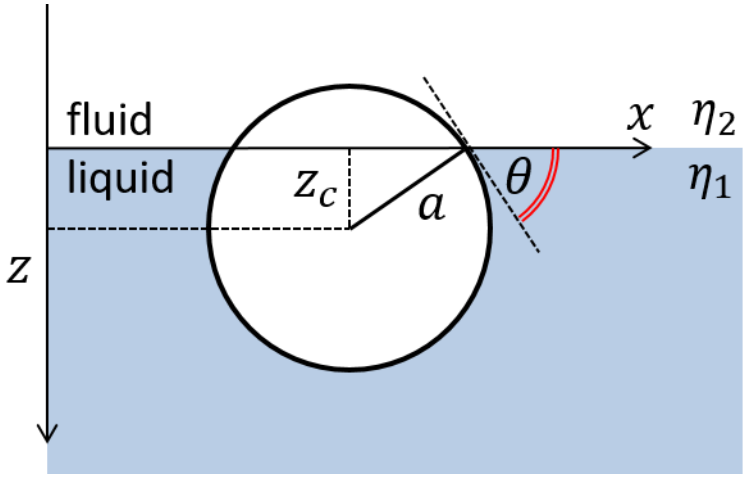

Figure 3: Sketch of a solid particle partially wetted at a liquid-fluid interface.

In more details, translational viscous drags at the interface have been quantitatively evaluated by hydrodynamic calculations. However, different assumptions should be made to achieve an analytical expression. Danov *et al.* [49] computed the pressure field and the local velocities for a particle partially immersed in a viscous incompressible fluid at low Reynolds and capillary numbers, in the contact angle θ range 30°-90°. The model considers lightweight particles only to prevent interface distortion induced by gravity. In this case, particle viscous drags depend only on the particle contact angle and the surface shear viscosity.

For heavyweight particles, gravity causes a curved meniscus, whose hydrodynamic resistance increases the drag above the bulk value [50].

Fischer *et al.* [6] numerically calculated the translational drag of a sphere at a flat interface assuming and incompressible interfacial flow ($\nabla_s \cdot u_s = 0$). The case of a flat interface leads also to the suppression of the rolling rotation of the sphere, in order to avoid any diverging tangential stress at the contact line. Translational viscous drag f of a particle moving parallel to a bare interface with an incompressible interfacial flow, normalized by bulk drag, writes as

$$f_{\parallel} = \frac{\zeta_{\parallel}^{T}}{\zeta_{\infty}^{T}} = \sqrt{\tanh[32(1+\cos\theta)/(9\pi^2)]}. \qquad (9)$$

Marangoni stress is also considered for an additional contribution due to surface shear viscosity, which scales linearly with Boussinesq number $\eta_s/a\eta_1$ (see section 2.3). In any cases, translational viscous drag parallel to the interface is lower than the bulk drag in the most viscous phase.

Pozrikidis [51] took into account the asymmetric distortion of a deformable interface due to the motion of the particle and numerically computed dimensionless translational drag coefficient parallel to the interface for some given values of the contact angle. Under the hypothesis of infinite viscosity ratio $\lambda = \eta_1/\eta_2$. ($\eta_1 >> \eta_2$) the mathematical problem can be simplified. Since the tangential stress at the interface has to be null, the interface can be treated as a symmetry plane. When the particle contact angle is θ = 90°, the Stokes flow is the same as in the bulk, and the translational viscous drag parallel to the interface is half the drag in bulk: $\zeta_{\parallel}^{T} = 3\pi\eta_1 a$, $f_{\parallel}$ = 0.5 [52][53][54]. Note that assumption of an incompressible interfacial flow leads to larger values of $f_{\parallel}$ =0.58 (see equation 9).

Zabarankin [55,56] extended the solution for hydrophilic particles (θ < 90°) by applying the same symmetry argument to a pair of fused sphere. The flow is computed for this new body, obtained by reflection of the immersed section of the sphere, and the numerical solutions were derived for a few contact angle values. Analytical expressions were later given by Dörr and Hardt for hydrophilic particles, θ < 90° [57][14]:

$$f_{\parallel} = \frac{1}{2}\left[1 + \frac{9}{16}\cos\theta - 0.139\cos^2\theta + O(\cos^3\theta)\right] \quad (10)$$

and for 90° < θ < 180° [14]:

$$f_{\parallel} = \frac{8}{9\pi}\sin\theta\left\{1 + \frac{\cot\theta/_2}{3\pi} + O\left[\cot^2\theta/_2\right]\right\} \quad (11)$$

In recent years, Koplik and Maldarelli [58,59] tackled the problem of a particle at the gas-liquid interface by molecular dynamics simulations, introducing a contribution of an interface with a finite thickness. All these approaches, both analytical and numerical, describing a particle attached to a free interface (in absence of surface viscosity), agree with a particle parallel drag smaller than the bulk value, $\zeta_{\parallel}^{T} < \zeta_{\infty}^{T}$, due to the partial particle immersion in the most viscous fluid. In all the studies presented so far, therefore, the dimensionless drag coefficient $f_{\parallel}(\theta) < 1$ for liquid-gas interfaces at any contact angle. Moreover, most of the models agree from a quantitative point of view (see figure 4), except for the model of Fischer *et al.* [6] that show a 15-20% higher translational drag due to the incompressible flow condition at the interface. For instance, at a contact angle θ = 45° $f_{\parallel} = 0.66$ [49][14], 0.67 [51], and $f_{\parallel} = 0.74$ for [6]. At θ = 90°, $f_{\parallel}$ = 0.5 for all the models, except Fischer *et al.*, $f_{\parallel} = 0.58$ [6]. At θ = 0, at $f_{\parallel} \approx 0.7$ (except Fischer *et al.*, $f_{\parallel} = 0.78$ [6]). At the limit θ = 180°, $f_{\parallel}$ tends to zero for al models, since the particle is immersed in the gas phase.

In a similar way, Navier-Stokes equations can be solved to estimate the drag when the particle is moving perpendicularly to the interface, i.e. along the vertical axis. O'Neill *et al.* [53] considered a half immersed spherical particle for infinity viscosity ratio ($\eta_1 >> \eta_2$), imposing null normal velocity and tangential stress as boundary conditions at the planar interface. Moreover, they hypothesized the existence of slip of the fluid along the submerged part of the sphere. The corresponding dimensionless drag coefficients ranges from $f_{\perp}$ = 0.47 for perfect slip up to $f_{\perp} \to \infty$ for non-slip condition. The latter can occur, for instance, when a strong contact line pinning inhibits the vertical motion of the particle. If we consider instead a realistic case of partial slip with a slip length of

the order of 1 nm, the dimensionless drag coefficient becomes size-dependent: $f_\perp$ = 3.11 for a = 1 μm and $f_\perp$ =1.19 if a = 10 nm. Note that these calculations include viscous terms only, and do not consider a specific drag due to the fluid boundary. Hence, if no external vertical forces are applied, the particle vertical Brownian motion at the interface is usually so highly confined that cannot be measured.

Considering again the simple case of infinite viscosity ratio $\lambda = \eta_1/\eta_2$. (η_1 >> η_2) and spherical particle with a contact angle θ = 90°, half of the bulk drag is also expected for the spinning rotational drag $\zeta_\parallel^R = 4\pi\eta a^3$ [53]. Note that as already stated before, a no slip boundary condition on the solid particle suppresses the rolling rotational motion, $\zeta_\perp^R = \infty$. Finite values of $\zeta_\perp^R$ were calculated by O'Neill *et al.* [53], who modelled rotational drags considering a finite slip length on the particle surface, which leads to $\zeta_\perp^R$ of the same order of magnitude as the bulk value for micrometric or nanometric particles [60]. Only the symmetric case θ = 90° at a free surface has been described by hydrodynamic models so far, and we are not aware of any predictions of $\zeta_\parallel^R$ and $\zeta_\perp^R$ as a function of θ.

When comparing hydrodynamic predictions to experiments, a very different behavior is observed for micrometric or nanometric particles at bare fluid interfaces. The models for the parallel translational drag catch the right tendency only for particles in the millimetric range [50] (black square points in figure 4). If we look at experimental results for particles of decreasing size down to few μm, these models start to underestimate the viscous contribution to the interfacial drag [61][62].

For hydrophilic particles (θ< 90°) the hydrodynamic theories predicted $f_\parallel$ = 0.66 – 0.75. In ref. [62][63] $f_\parallel$ = 0.83. Enhanced $f_\parallel$ drag is much more evident for nanoparticles [64][65][66][67]. In particular, Wang *et al.* [65] measured the dynamics of 10-20 nm quantum dots (QDs) at water-alkanes interfaces. The measured dimensionless drag coefficient is $f_\parallel$ = 1.5 for hydrophilic QDs and $f_\parallel$ = 2 for hydrophobic ones (no details are provided for contact angles) (purple bars in figure 4). In figure 4, one can note not only the anomalously large values for interfacial drag, but also its increase with contact angle. In other words, less the particle is immersed in the most viscous phase (water, in the case of water-alkanes interfaces), larger is the interfacial drag.

Boniello *et al.* [15] performed a first systematic study on the interfacial drag of micrometric spherical particles as a function of their immersion. By surface functionalization, the static particle contact angle of the particles was varied in the range between 30° and 130°. Experiments were performed on a clean air-water interface in a very diluted particle density regime. Hydrophilic beads show a dimensionless translational drag coefficient of the around $f_\parallel$ = 0.83: lower than the value in bulk water, but not as low as predicted by analytical and numerical calculations [6][49][51][58]. Moreover, $f_\parallel$ seems to be quite insensitive to the contact angle, keeping a slightly constant value. For hydrophobic particles $f_\parallel$ strongly increases; translational drag at the interface overcomes the drag in the bulk despite the decreasing immersion in the liquid of the particles (and more exposure to the gas). The same qualitative behavior is observed for spheroidal particles too [68]. This study shows a significant dependency on the aspect ratio: for comparable wetting, the most anisotropic particles have the largest drag. The dimensionless drag coefficient reaches $f_\parallel \approx$ 1.5 for translational dynamics and $g_\parallel = \frac{\zeta_\parallel^R}{\zeta_\infty^R} \approx$ 5-6 for spinning rotational one at the largest aspect ratio ($\Phi \approx 10$). Note that typical quadrupolar distortion of the interface around a spheroidal particle [69] is not sufficient to explain the variation of dissipation, reminiscently with the argument of Petkov *et al.* [50] for heavy beads. In fact, the altitude difference between the depressions at the tips and the raises at the particle sides

accounts approximately 10% of the size of the particle at the maximum experimental aspect ratio value ($\Phi \approx 10$). Rotational drag coefficients $g_{\parallel}$ and $g_{\perp} = \frac{\zeta_{\perp}^{R}}{\zeta_{\infty}^{R}}$ were also measured for Janus spherical particles, $\theta \approx 65°$ at the water-air interface: $g_{\parallel}$= 2.4-12 and $g_{\perp}$= 14-87, which cannot be described by the hydrodynamic models cited before [60].

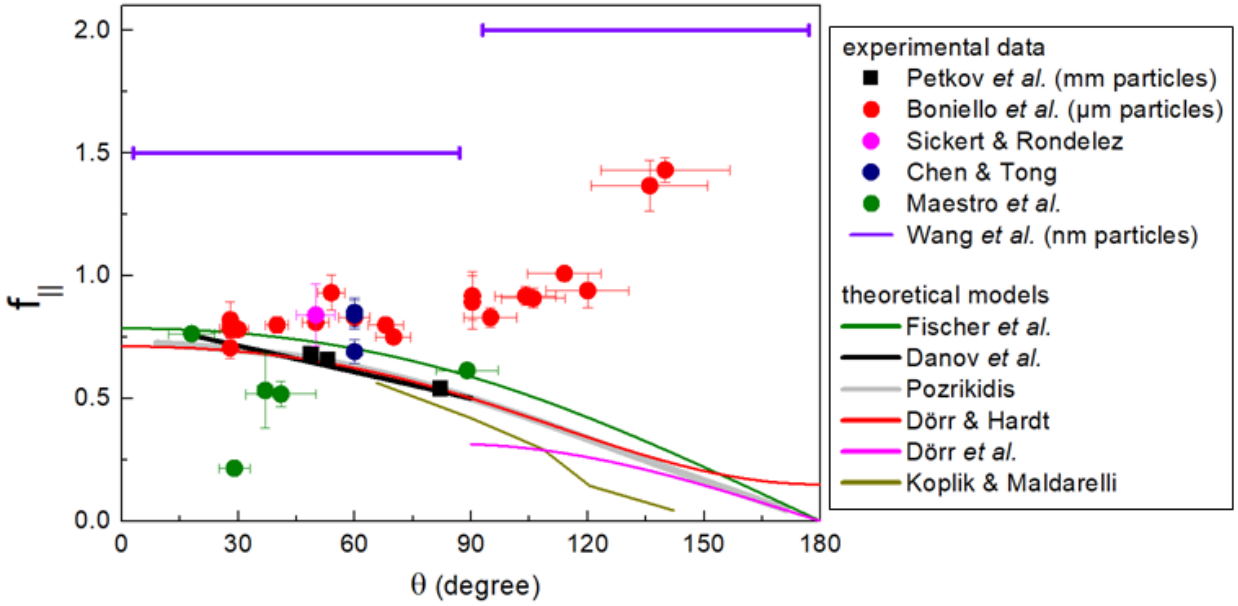

Figure 4: Dimensionless translational drag coefficient at the interface $f_{\parallel}$, defined as the ratio between interfacial and bulk drags, as a function of the particle contact angle, from recent literature [50][15][61][62][70][65]. Points show experimental measurements for particle sizes of the order of mm (square) and μm (circles). Purple bars represents values for nanoparticles from [65] (contact angle not reported). Solid lines represent theoretical models: Fischer *et al.* [6] (green line), Danov *et al.* [49], Pozrikidis [51], Dörr & Hardt [57] (black, gray and red line, superposed in the graph); asymptotic model from Dörr *et al.* [71] (magenta line); simulation Koplik & Maldarelli [58] (olive line).

2.2. The *unexpected* key importance of capillary effects on particle motion

Experimental measurements shown in figure 4 demonstrate that hydrodynamic modeling of the translational interfacial drag is incomplete. It is applicable for macroscopic particles, but it loses its validity for smaller sizes (radius ~ μm - nm). Arguments based on a limited number of molecular collisions in the gas phase or the elastic response of the interface [72] are not suitable to explain the observed dynamics. Indeed, diffusion in bulk gases is faster than diffusion in liquids, despite fewer molecular collisions (or because of them, since they are responsible of viscous drag). Elastic confinement parallel at the interface, besides the fact that is not experimentally observed in any work, violates the translational invariance of the interface on its plane [73]. Hydrodynamics resistance associated to curved menisci offers just a partial contribution to enhanced viscous drag. Finite element simulations [74] indicate an upper bound limit of 10% variation of interfacial drag due to distortions, much lower than the typically observed variation at air-liquid interfaces.

To fill this gap between experimental observations and predicted values, Boniello *et al.* proposed to explain the enhanced parallel translational drag by a mechanism that involves fluctuations of the interface at the contact line [15]. Irregular undulations of the interface and continuous pinning and depinning of the contact line on surface

defects cause capillary random forces acting on the particle. The overall effect of these uncorrelated forces translates in an additional drag. The fact that such a source of dissipation lies on the interface and is related to the contact line agrees with some peculiarities observed above. In particular, vertical fluctuations are more relevant for smaller colloids (nanoparticles), when the drag induced by interface fluctuations at the contact line can overcome the known viscous drag. Expressions for the rotational drags due fluctuations of the interface at the contact line were also given by Stocco *et al.* to explain the rotational diffusions of Janus microparticles at the liquid-gas interface [60].

The limitation of this model is the absence of experimental evidence of nano- or subnano- metric fluctuations at the contact line. State of art experiments do not allow to have access to both spatial (≈nm) and temporal (≈ps-ns) resolution of contact line fluctuations. However, some indirect confirmations have been found for nanoscaled defects.

Ondarçuhu and Piednoir followed by atomic force microscopy (AFM) the dewetting of polystyrene films on a terraced substrate with nanometric steps [75]. Pinning occurs and affects contact line dynamics in different ways when it is moving upward or downward the steps. The surface can be considered completely smooth only when heterogeneities are smaller than the size of fluid molecules.

Surface heterogeneities and roughness distort the contact line at the nanoscale, but this is sufficient to induce capillary interactions between particles [76][77][78], in the same way as curved menisci around anisotropic particles do [69].

Contact line pinning is also responsible for the slow relaxation dynamics during particle adsorption. Kaz *et al.* [48] observed a slow logarithmic particle vertical displacement with time between the breach of the interface and the equilibrium position. This vertical motion cannot be described by viscous dissipations or by capillary waves, but it can be explained by the dynamics of interfacial forces on the contact line. Such forces alter the rate of thermal hopping of the contact line between pinning sites. The driving force of the vertical motion decreases moving toward the equilibrium contact angle, which leads to a characteristic logarithmic motion relaxation. Typical pinning sites are related to topological features, such as surface roughness or the presence of chemical heterogeneities [48][79].

Tong and coworker used AFM on a cylindrical fiber moving perpendicularly to the interface to explore the effect of fluid motion in the immediate vicinity of the contact line [80]. In this way they were able to direct measure a dissipation on the vertical motion induced by the fluctuating contact line.

Giacomello *et al.* [81] calculated that nanodefects are able to create metastable pinned states where depinning can be thermally activated in absence of driving forces. From a mathematical point of view, it has been shown that the presence of defects on a heterogeneous surface introduces perturbation mode of the contact line, whose response function has been derived [82].

These observations provide evidences for a contact line dynamics contribution to the motion of micro- and nano-particles at fluid interfaces. If, on the one hand, capillary dynamics effects allow to understand enhanced translational and rotational drag and could be a tool to tune particle mobility, on the other hand they increase the number of unknown parameters in surface microrheology, which uses colloidal particles at the interface as probes of the interfacial viscoelasticity. First of all, it would not be easy to relate translational diffusion coefficient

(measured by particle tracking) and interfacial shear viscosity, since it depends also on contact line pinning on the particle. Preliminary calibrations of the colloidal probe on bare interfaces may be not sufficient to evaluate the contact line dynamics contribution to the translational drag, since the latter depends also on the interfacial tension and local viscosity. Secondly, the interaction between the probe particle and the surface active species at the contact line may significantly perturb the probe boundary conditions, the interface structure and properties, which may render this method highly perturbative [83].

2.3. Surface microrheology

Studying the motion of micro- and nano-particles at the fluid interface can provide important information on the viscoelastic properties of the interface, which can be regarded not as a purely two dimensional system but as a thin region between two macroscopic fluids, see figure 5. Even in absence of any surface active species, one can define a thickness of the interfacial region, which is usually smaller than a nanometer if one considers the amplitude of capillary waves or the intrinsic interfacial profile [84]. For surfactant monolayers and lipid bilayers, an interfacial thickness corresponding to the size of the surfactants of the order of few nanometers can be defined. This thickness can extend to few tens of nm or more for protein layers or when considering nanoparticle and colloid monolayers. In 1.2, we have already introduced the dilatational (η_d) and the shear (η_s) interfacial viscosities, which describe the in-plane dissipations occurring if the interfacial area is changed or if a shear stress is applied in the interfacial plane respectively [33], see figure 5.

As discussed before for the parallel translational motion of particles attached to the interface, the dilatational viscosity may play a role in the particle motion if the front of the particle is able to compress the interfacial area populated by surface active species (and expand the interfacial area on the rear of the particle). Usually, this compression cannot take place since the surface active species move much faster than the particle. Hence the effect of η_d is usually negligible as pointed out by T. Fischer [6][85]. However, for polymer monolayers a compression-dilatation dissipation may occur given that the polymer diffusion can be comparable to the particle diffusion. A model built for soluble surfactant monolayers, for which molecules can exchange between the interface and the bulk, provides an expression for the dilatational viscosity [86]:

$$\eta_d = \frac{K_d}{\nu}\frac{\sqrt{\nu_d/\nu}}{1+2\sqrt{\nu_d/\nu}+2\nu_d/\nu}\,, \qquad (12)$$

where K_d is the elastic compression modulus, and ν_d is the characteristic frequency of the diffusional matter exchange [87]. In the equation 12, η_d is not a constant but it decreases if the frequency increases. An additional intrinsic dilatational viscosity should also be taken into account to describe the dissipation occurring even in absence of matter exchange as pointed out by D. Langevin [86]. It is also important to remark that surface viscosities are excess quantities, which means that a zero value of a surface viscosity corresponds to non-zero local viscosity (surface viscosity × interface thickness = local viscosity – bare viscosity), which is the same as the one of the bare interface [86]. For surfactant monolayers, positive and negative η_d have been measured in a large range of frequencies ($10^{-2} < \nu < 10^{6}$ s^{-1}): $\eta_d\nu \approx$ –10 - +10 10^{-3} N.m^{-1} [88][89][90]. For polymer monolayers, experimental values of η_d varies strongly with ν: , $\eta_d \approx 1$ N.s.m^{-1} for $\nu < 10^{-3}$ s^{-1} (measured by oscillatory barrier tensiometry) and $\eta_d \approx 10^{-7}$ N.s.m^{-1} for $10^{5} < \nu < 10^{6}$ s^{-1} (by surface light scattering) [91].

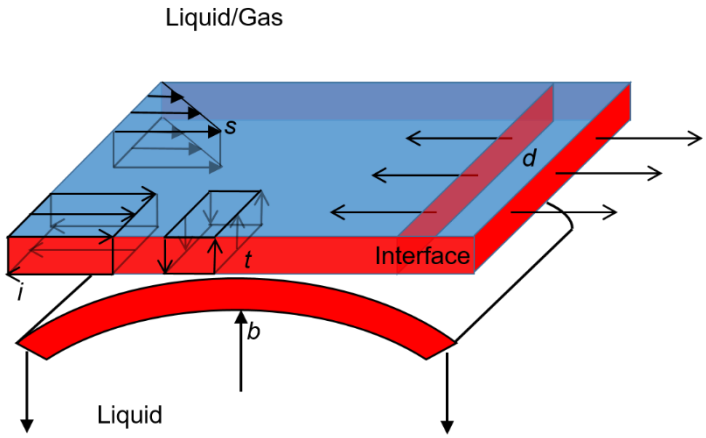

Figure 5: Sketch of an interface with a defined thickness in between two fluids and the corresponding dissipation surface modes: dilatation (d), shear (s), transverse (t), bending (b) and interlayer

Typical surface shear viscosities evaluated by measuring the parallel translational diffusion of partially wetted microparticles are: $\eta_s = 10^{-10}$ - 10^{-7} N.s.m^{-1} for polymer monolayers [92], and $\eta_s \approx 10^{-9}$ N.s.m^{-1} for surfactant monolayers [6]. Hence, η_d and η_s values are very similar, which may explain why for fatty acid monolayers Fischer's (incompressible interface [6]) and Danov's (compressible interface [49]) models provide very similar η_s results [63].

Now going back to figure 4, which reports the parallel translational drag for partially wetted particles at bare interfaces, we can estimate a range of values for the surface shear viscosity, $0 < \eta_s < 5\times10^{-9}$ N.s.m^{-1} that would fit the experimental data and can be considered the limiting accuracy of surface microrheology by microparticle tracking. Indeed a surface shear viscosity as low as $\eta_s \approx 5\times10^{-9}$ N.s.m^{-1} cannot be measured by tracking the translational motion of colloidal particles at the interface since the particle may experience a drag due to contact line fluctuations, which would correspond to $\eta_s \approx 5\times10^{-9}$ N.s.m^{-1}. Given that η_d and η_s described before are very close to the accuracy of passive surface microrheology, a safer strategy to measure surface viscosities is to increase the Boussinesq numbers $n_d = \eta_d/a\eta_1$ and $n_s = \eta_s/a\eta_1$, in order to minimize the bulk contributions to the drag. The best way to obtain $n_d = \eta_d/a\eta_1 > 1$ and $n_s = \eta_s/a\eta_1 > 1$, is to reduce the probe size a.

Dhar *et al.* [93] for instance use a magnetic nanorod to probe the surface viscosity of proteins at the air-water interface. They measure the rod reorientation from perpendicular to parallel to the applied magnetic field, which is connected to the spinning rotation at the interface. Hence, they were able to evaluate η_s in the range between10^{-9} N.s.m^{-1} and 10^{-5} N.s.m^{-1} [93]. Active microrheology can be also performed tracking the orientation of a self-propelled particle probe [94]. Commercially available and new developments of active surface micro rheometers, called interfacial stress rheometry, are based on tracking the parallel translational motion of magnetic needles at the interface. They are also using probes of smaller sizes toward the submicron scale in order to increase sensitivity and accuracy [33].

Other dissipation modes could be defined for an interfacial layer between two macroscopic fluid phases. For interfaces with significant interfacial tensions, $\sigma > 10^{-3}$ N/m, one can introduce a transverse viscosity (η_t) connected to the shear normal to the surface. From a rheological perspective, this transverse shear is governed by a complex interfacial tension $\sigma + i\nu\eta_t$ as discussed in surface light scattering studies [95]. For fatty acid monolayers, η_t =10^{-9} - 10^{-8} N.s.m^{-1} was measured by capillary wave scattering, which points to the importance of this viscosity only at large values of the frequency, $\nu > 10^5$ s^{-1} [96][97]. Hence, the transverse viscosity could also play a role in the vertical motion of partially wetted particles in the presence of surfactants at high frequencies. These frequencies can be imposed by external forces as in optical tweezers or in colloidal probe AFM experiments.

Note that for thermal Brownian motion, a unique frequency cannot be defined. One could consider a frequency from the momentum relaxation time for translational Brownian motion, which describes the time necessary to lose momentum due to viscous dissipation in the fluid: $\tau_{mr} = \frac{m}{\zeta_\infty^T} = \frac{2\rho}{9\eta}a^2$ (m is the particle mass and ρ the particle density) for spherical particle in the bulk, which leads to a frequency $\nu = \tau_{mr}^{-1} \approx 10^6$ s^{-1} (10^8 s^{-1}) for a= 2 µm (0.2 µm). Other frequencies can be defined in the generalized Stokes–Einstein equation by the lag time of the mean squared displacement, which typically gives 10^{-2} s^{-1}< ν < 10^2 s^{-1} [92].

Finally, we want to briefly introduce two additional dissipation modes which are important for very low interfacial tension systems, σ < 10^{-3} N/m, such as in floating supported lipid bilayers or in giant unilamellar vesicles. Microparticle and nanoparticle interactions with those interfaces play very important roles in drug delivery, cancer therapy, endocytosis and diagnostics given that cell membranes in many organisms is composed by lipid bilayers [98]. These low interfacial tension interfaces may show large fluctuations and two dissipation modes must be taken into account: interlayer and bending, associated to a sliding occurring inside the interfacial layer and the change of the interface curvature ΔC respectively, see Figure 5 [99,100].

The interlayer dissipation describes the inner friction of the interface when a lateral shear leads to a sliding between the top and the bottom monolayer in a bilayer. This sliding may result from a mismatch of the lateral monolayer relaxations after a sudden bending of the bilayer, and involves a friction between the hydrophobic chains of the top monolayer with the ones of the bottom monolayer [99][101]. For bilayers, typical values of the interlayer friction coefficient b (dimension of a 3D viscosity/length) are in the range b = 10^6 - 10^8 Pa.s.m^{-1} [99][102], which correspond to local 3D viscosity ≈10^{-3} - 10^{-1} Pa.s [99]. Recently, particle tracking of a membrane-adhering vesicle was used to evaluate the interlayer friction of a supported lipid bilayer, b = 10^7 Pa.s.m^{-1} [103].

As all the other modes, bending is characterized by both an elastic and a viscous components. In the literature, only the bending elastic modulus K_b is usually described, $M = K_b\Delta C$ (where M is the surface bending moment) and for phospholipid bilayers K_b≈ 10^{-19} N.m [104]. The viscous bending moment can be written as $M = \eta_b \frac{\partial \Delta C}{\partial t}$ [100]. It may play a major role in the dynamics of nanoparticle engulfment, which is controlled by the adhesion strength and the membrane bending. The membrane wraps the particle either partially or completely if the adhesion is stronger than the bending resistance. In principle, during the engulfment dynamics, the bending viscosity may play a role in particular when $\frac{\partial \Delta C}{\partial t}$ is small. This case could be encounter in the engulfment of a particle by a lipid vesicle with comparable sizes, showing low changes of the interface curvature ΔC.

Conclusions

In this review we aim at summarising models and experimental results on the motion of colloidal particles either in the neighbourhood or attached to a fluid interface. The interface can be bare or populated by surface active species ranging from ions to macromolecules. In any case, it will be never clean: in the sense that molecules at the interface are different from the bulk molecules because they feel different interactions even for pure fluid phases. For a particle moving in the proximity of a fluid interface, if the gap distance between the particle and interface is reduced to the nm scale, a mutual interaction between the solid particle and the fluid interface take place. In the region between the solid and the fluid, a liquid gap has the difficult task to accommodate the transition of physical (*e.g.* dielectric constant) and chemical (*e.g.* pH) properties, which are very different in the solid (particle) and in the fluid. This transition region is also responsible for the hydrodynamic boundary conditions which play a major roles in the rotational and translational motion of the solid particle. A colloidal particle translating and/or rotating very close or attached to a fluid interface feel these interfacial profiles and they can be used as local probes of surface interactions and surface viscosities. The motion of colloidal particles may also perturb these interfacial profiles, and the fluid interface may counteract showing dissipation modes that are present only at the interface (e.g bending or interlayer) and not in the bulk.

To conclude, we strongly believe that beyond hydrodynamics, many other effects due to dissipation modes of the surface or related to electrokinetic effects can be investigated in future experiments using nano- or micro-particle very close or attached to a fluid interface.

Acknowledgement

We gratefully acknowledge the financial support of ANR Surfanicol (ANR14-CE07-0039-01) and Labex Numev (n° 2014-2-44).

References

[1] Y. Chevalier, M.A. Bolzinger, Emulsions stabilized with solid nanoparticles: Pickering emulsions, Colloids Surfaces A Physicochem. Eng. Asp. 439 (2013) 23–34. doi:10.1016/j.colsurfa.2013.02.054.

[2] S. Lam, K.P. Velikov, O.D. Velev, Pickering stabilization of foams and emulsions with particles of biological origin, Curr. Opin. Colloid Interface Sci. 19 (2014) 490–500. doi:10.1016/j.cocis.2014.07.003.

[3] D. Lopez, E. Lauga, Dynamics of swimming bacteria at complex interfaces, Phys. Fluids. 26 (2014). doi:10.1063/1.4887255.

[4] R. McGorty, J. Fung, D. Kaz, V.N. Manoharan, Colloidal self-assembly at an interface, Mater. Today. 13 (2010) 34–42. doi:10.1016/S1369-7021(10)70107-3.

[5] K.D. Danov, T.D. Gurkov, H. Raszillier, F. Durst, Stokes flow caused by the motion of a rigid sphere close to a viscous interface, Chem. Eng. Sci. 53 (1998) 3413–3434. doi:10.1016/S0009-2509(98)00137-7.

[6] T.M. Fischer, P. Dhar, P. Heinig, The viscous drag of spheres and filaments moving in membranes or monolayers, J. Fluid Mech. 558 (2006) 451. doi:10.1017/S002211200600022X.

[7] T. Bickel, J.C. Loudet, G. Koleski, B. Pouligny, Hydrodynamic response of a surfactant-laden interface to a radial flow, Phys. Rev. Fluids. 4 (2019). doi:10.1103/PhysRevFluids.4.124002.

[8] T. Bickel, Effect of surface-active contaminants on radial thermocapillary flows, Eur. Phys. J. E. 42 (2019). doi:10.1140/epje/i2019-11896-5.

[9] A. Maali, R. Boisgard, H. Chraibi, Z. Zhang, H. Kellay, A. Würger, Viscoelastic Drag Forces and Crossover from No-Slip to Slip Boundary Conditions for Flow near Air-Water Interfaces, Phys. Rev. Lett. 118 (2017). doi:10.1103/PhysRevLett.118.084501.

[10] G.M. Wang, R. Prabhakar, E.M. Sevick, Hydrodynamic Mobility of an Optically Trapped Colloidal Particle near Fluid-Fluid Interfaces, Phys. Rev. Lett. 103 (2009) 1–4. doi:10.1103/PhysRevLett.103.248303.

[11] T. Watarai, T. Iwai, Experimental study on air-liquid interface effect of Brownian dynamics using spectral-domain low-coherence dynamic light scattering, Opt. Rev. 21 (2014) 378–381. doi:10.1007/s10043-014-0058-1.

[12] A. Stocco, T. Mokhtari, G. Haseloff, A. Erbe, R. Sigel, Evanescent-wave dynamic light scattering at an oil-water interface: Diffusion of interface-adsorbed colloids, Phys. Rev. E. 83 (2011) 1–11. doi:10.1103/PhysRevE.83.011601.

[13] J.C. Benavides-Parra, D. Jacinto-Méndez, G. Brotons, M.D. Carbajal-Tinoco, Brownian motion near a liquid-gas interface, J. Chem. Phys. 145 (2016). doi:10.1063/1.4962746.

[14] D. Aaron, S. Hardt, H. Masiud, H. Stone, Drag and diffusion coefficients of a spherical particle attached to a fluid interface, J. Fluid Mech. 790 (2016) 607–618. doi:10.1017/jfm.2016.41.

[15] G. Boniello, C. Blanc, D. Fedorenko, M. Medfai, N. Mbarek, M. In, M. Gross, A. Stocco, M. Nobili, Brownian diffusion of a partially wetted colloid, Nat. Mater. (2015) Doi:10.1038/nmat4348.

[16] R. Shlomovitz, A.A. Evans, T. Boatwright, M. Dennin, A.J. Levine, Measurement of monolayer viscosity using noncontact microrheology, Phys. Rev. Lett. 110 (2013) 29–33. doi:10.1103/PhysRevLett.110.137802.

[17] L.D. Landau, E.M. Lifshitz, Landau and Lifshitz 6: Fluid mechanics, Image Rochester NY. 6 (1987) 539. doi:10.1007/b138775.

[18] H. Brenner, The slow motion of a sphere through a viscous fluid towards a plane surface, Chem. Eng. Sci. 16 (1961) 242–251. doi:10.1016/0009-2509(61)80035-3.

[19] A.J. Goldmant, R.G. Cox, H. Brenner, A.J. Goldman, Slow viscous motion of a sphere parallel to a plane wall II Couette flow, Chem. Eng. Sci. 22 (1967) 653.

[20] A. V Nguyen, G.M. Evans, Exact and global rational approximate expressions for resistance coefficients for a colloidal solid sphere moving in a quiescent liquid parallel to a slip gas-liquid interface., J. Colloid Interface Sci. 273 (2004) 262–70. doi:10.1016/j.jcis.2003.12.044.

[21] B.S.H. Lee, R.S. Chadwickt, L.G. Leal, Motion of a sphere in the presence of a plane interface . Part 1 . An approximate solution by generalization of the method of Lorentz, J. Fluid Mech. 93 (1979) 705–726.

[22] S.H. Lee, L.G. Leal, Motion of a sphere in the presence of a plane interface. Part 2. An exact solution in bipolar co-ordinates, J. Fluid Mech. 98 (1980) 193. doi:10.1017/S0022112080000109.

[23] J. V Boussinesq, Sur l'existence d'une viscosite superficielle, dans la mince couche de transition separant un liquide d'un autre fluide contigu, Ann. Chim. Phys. 29 (1913) 349–362.

[24] L.E. Scriven, Dynamics of a Fluid Interface, Chem. Eng. Sci. 12 (1960) 98–108. doi:10.1016/0009-2509(60)87003-0.

[25] A.M.J. Davis, M.E. O'Neill, The slow rotation of a sphere submerged in a fluid with a surfactant surface layer, Int. J. Multiph. Flow. 5 (1979) 413–425. doi:10.1016/0301-9322(79)90029-6.

[26] J. Bławzdziewicz, M.L. Ekiel-Jeewska, E. Wajnryb, Motion of a spherical particle near a planar fluid-fluid interface: The effect of surface incompressibility, J. Chem. Phys. 133 (2010). doi:10.1063/1.3475197.

[27] G.D.M. MacKay, S.G. Mason, Approach of a solid sphere to a rigid plane interface, J. Colloid Sci. 16 (1961) 632–635. doi:10.1016/0095-8522(61)90049-6.

[28] L. Arauz-lara, M.D. Carbajal-tinoco, R. Lopez-fernandez, Asymmetry in Colloidal Diffusion near a Rigid Wall D (h), 138303 (2007) 1–4. doi:10.1103/PhysRevLett.99.138303.

[29] K. Ishii, T. Iwai, H. Xia, Hydrodynamic measurement of Brownian particles at a liquid-solid interface by low-coherence dynamic light scattering, Opt. Express. 18 (2010) 7390. doi:10.1364/oe.18.007390.

[30] L. Liu, A. Woolf, A.W. Rodriguez, F. Capasso, Absolute position total internal reflection microscopy with an optical tweezer, Proc. Natl. Acad. Sci. U. S. A. 111 (2014) E5609–E5615. doi:10.1073/pnas.1422178112.

[31] C. Ha, H.D. Ou-Yang, H.K. Pak, Direct measurements of colloidal hydrodynamics near flat boundaries using oscillating optical tweezers, Phys. A Stat. Mech. Its Appl. 392 (2013) 3497–3504. doi:10.1016/j.physa.2013.04.014.

[32] R. Shlomovitz, A. a. Evans, T. Boatwright, M. Dennin, A.J. Levine, Measurement of Monolayer Viscosity Using Noncontact Microrheology, Phys. Rev. Lett. 110 (2013) 137802. doi:10.1103/PhysRevLett.110.137802.

[33] E. Guzmán, J. Tajuelo, J.M. Pastor, M.Á. Rubio, F. Ortega, R.G. Rubio, Shear rheology of fluid interfaces: Closing the gap between macro- and micro-rheology, Curr. Opin. Colloid Interface Sci. 37 (2018) 33–48. doi:10.1016/j.cocis.2018.05.004.

[34] R. Shlomovitz, A.A. Evans, T. Boatwright, M. Dennin, A.J. Levine, Probing interfacial dynamics and mechanics using submerged particle microrheology. I. Theory, Phys. Fluids. 26 (2014). doi:10.1063/1.4886996.

[35] T. Boatwright, M. Dennin, R. Shlomovitz, A.A. Evans, A.J. Levine, Probing interfacial dynamics and mechanics using submerged particle microrheology. II. Experiment, Phys. Fluids. 26 (2014). doi:10.1063/1.4887084.

[36] R.A. Pushkarova, R.G. Horn, Bubble-solid interactions in water and electrolyte solutions, Langmuir. 24 (2008) 8726–8734. doi:10.1021/la8007156.

[37] P. Warszyński, Coupling of hydrodynamic and electric interactions in adsorption of colloidal particles, Adv. Colloid Interface Sci. 84 (2000) 47–142. doi:10.1016/S0001-8686(99)00015-9.

[38] H. Ohshima, T.W. Healy, L.R. White, R.W. O'Brien, Sedimentation velocity and potential in a dilute suspension of charged spherical colloidal particles, J. Chem. Soc. Faraday Trans. 2 Mol. Chem. Phys. 80 (1984) 1299–1317. doi:10.1039/F29848001299.

[39] S.M. Tabatabaei, T.G.M. van de Ven, A.D. Rey, Electroviscous sphere-wall interactions, J. Colloid Interface Sci. 301 (2006) 291–301. doi:10.1016/j.jcis.2006.04.047.

[40] D.C. Prieve, S.G. Bike, Electrokinetic Repulsion Between Two Charged Bodies Undergoing Sliding Motion, Chem. Eng. Commun. 55 (1987) 149–164. doi:10.1080/00986448708911924.

[41] R.G. Cox, T.G.M. Van De Ven, Electroviscous forces on a charged particle suspended in a flowing liquid, J. Fluid Mech. 338 (1997) 1–34. doi:10.1017/S0022112097004862.

[42] P. Warszyński, X. Wu, T.G.M. Van De Ven, Electrokinetic lift force for a charged particle moving near a charged wall - A modified theory and experiment, in: Colloids Surfaces A Physicochem. Eng. Asp., 1998: pp. 183–198. doi:10.1016/S0927-7757(97)00277-X.

[43] S. Bianchi, F. Saglimbeni, G. Frangipane, D. Dell'Arciprete, R. Di Leonardo, 3D dynamics of bacteria wall entrapment at a water-air interface, Soft Matter. 15 (2019) 3397–3406. doi:10.1039/c9sm00077a.

[44] O. Manor, I.U. Vakarelski, X. Tang, S.J. O'Shea, G.W. Stevens, F. Grieser, R.R. Dagastine, D.Y.C. Chan, Hydrodynamic boundary conditions and dynamic forces between bubbles and surfaces, Phys. Rev. Lett. 101 (2008). doi:10.1103/PhysRevLett.101.024501.

[45] O. Manor, I.U. Vakarelski, G.W. Stevens, F. Grieser, R.R. Dagastine, D.Y.C. Chan, Dynamic

forces between bubbles and surfaces and hydrodynamic boundary conditions, Langmuir. 24 (2008) 11533–11543. doi:10.1021/la802206q.

[46] P. Pieranski, Two-Dimensional Interfacial colloidal crystal, Phys. Rev. Lett. 45 (1980) 569.

[47] A. Stocco, M. Nobili, A comparison between liquid drops and solid particles in partial wetting, Adv. Colloid Interface Sci. 247 (2017) 223–233. doi:10.1016/j.cis.2017.06.014.

[48] D.M. Kaz, R. McGorty, M. Mani, M.P. Brenner, V.N. Manoharan, Physical ageing of the contact line on colloidal particles at liquid interfaces., Nat. Mater. 11 (2012) 138–42. doi:10.1038/nmat3190.

[49] K. Danov, R. Aust, F. Durst, U. Lange, Influence of the surface viscosity on the hydrodynamic resistance and surface diffusivity of a large brownian particle, J. Colloid Interface Sci. 175 (1995) 36–45. doi:10.1006/jcis.1995.1426.

[50] J.T. Petkov, N.D. Denkov, K. Danov, O.D. Velev, R. Aust, F. Durst, Measurement of the Drag Coefficient of Spherical Particles attached to Fluid Interfaces, J. Colloid Interface Sci. 172 (1995) 147–154.

[51] C. Pozrikidis, Particle motion near and inside an interface, J. Fluid Mech. 575 (2007) 333. doi:10.1017/S0022112006004046.

[52] K.B. Ranger, The circular disk straddling the interface of a two-phase flow, Int. J. Multiph. Flow. 4 (1978) 263–277. doi:10.1016/0301-9322(78)90002-2.

[53] M.E. O'Neill, K.B. Ranger, H. Brenner, Slip at the surface of a translating–rotating sphere bisected by a free surface bounding a semi-infinite viscous fluid: Removal of the contact-line singularity, Phys. Fluids. 29 (1986) 913. doi:10.1063/1.865686.

[54] B. Radoev, V. Djakovichi, Brownian Motion at Liquid-Gas Interfaces. 1. Diffusion Coefficients of Macroparticles at Pure Interfaces, Langmuir. (1992) 2962–2965.

[55] M. Zabarankin, Asymmetric three-dimensional Stokes flows about two fused equal spheres, Proc. R. Soc. A Math. Phys. Eng. Sci. 463 (2007) 2329–2349. doi:10.1098/rspa.2007.1872.

[56] M. Zabarankin, Correction for Zabarankin, Asymmetric three-dimensional Stokes flows about two fused equal spheres, Proc. R. Soc. A Math. Phys. Eng. Sci. 463 (2007) 3396–3396. doi:10.1098/rspa.2007.2003.

[57] A. Dörr, S. Hardt, Driven particles at fluid interfaces acting as capillary dipoles, J. Fluid Mech. 770 (2015) 5–26. doi:10.1017/jfm.2015.129.

[58] J. Koplik, C. Maldarelli, Diffusivity and hydrodynamic drag of nanoparticles at a vapor-liquid interface, Phys. Rev. Fluids. 2 (2017). doi:10.1103/PhysRevFluids.2.024303.

[59] J. Koplik, C. Maldarelli, Molecular dynamics study of the translation and rotation of amphiphilic Janus nanoparticles at a vapor-liquid surface, Phys. Rev. Fluids. 4 (2019). doi:10.1103/PhysRevFluids.4.044201.

[60] A. Stocco, B. Chollet, X. Wang, C. Blanc, M. Nobili, Rotational diffusion of partially wetted colloids at fluid interfaces, J. Colloid Interface Sci. 542 (2019) 363–369. doi:10.1016/j.jcis.2019.02.017.

[61] M. Sickert, F. Rondelez, Shear Viscosity of Langmuir Monolayers in the Low-Density Limit, Phys. Rev. Lett. 90 (2003) 126104. doi:10.1103/PhysRevLett.90.126104.

[62] W. Chen, P. Tong, Short-time self-diffusion of weakly charged silica spheres at aqueous interfaces, EPL (Europhysics Lett. 84 (2008) 28003. doi:10.1209/0295-5075/84/28003.

[63] M. Sickert, F. Rondelez, H. a. Stone, Single-particle Brownian dynamics for characterizing the rheology of fluid Langmuir monolayers, Europhys. Lett. 79 (2007) 66005. doi:10.1209/0295-5075/79/66005.

[64] K. Du, J.A. Liddle, A.J. Berglund, Three-dimensional real-time tracking of nanoparticles at an oil-water interface., Langmuir. 28 (2012) 9181–8. doi:10.1021/la300292r.

[65] D. Wang, S. Yordanov, H.M. Paroor, A. Mukhopadhyay, C.Y. Li, H.-J. Butt, K. Koynov, Probing diffusion of single nanoparticles at water-oil interfaces., Small. 7 (2011) 3502–7. doi:10.1002/smll.201101823.

[66] T. Gehring, T.M. Fischer, Diffusion of Nanoparticles at an Air/Water Interface Is Not Invariant under a Reversal of the Particle Charge, J. Phys. Chem. C. 115 (2011) 23677–23681. doi:10.1021/jp2061738.

[67] D. Wang, R. Hu, M.J. Skaug, D.K. Schwartz, Temporally anticorrelated motion of nanoparticles at a liquid interface, J. Phys. Chem. Lett. 6 (2015) 54–59. doi:10.1021/jz502210c.

[68] G. Boniello, A. Stocco, M. Gross, M. In, C. Blanc, M. Nobili, Translational viscous drags of an ellipsoid straddling an interface between two fluids, Phys. Rev. E. 94 (2016) 012602. doi:10.1103/PhysRevE.94.012602.

[69] J. Loudet, a. Yodh, B. Pouligny, Wetting and Contact Lines of Micrometer-Sized Ellipsoids, Phys. Rev. Lett. 97 (2006) 1–4. doi:10.1103/PhysRevLett.97.018304.

[70] A. Maestro, L.J. Bonales, H. Ritacco, T.M. Fischer, R.G. Rubio, F. Ortega, Surface rheology: Macro- and microrheology of poly(tert-butyl acrylate) monolayers, Soft Matter. 7 (2011) 7761–7771. doi:10.1039/c1sm05225j.

[71] A. Dörr, S. Hardt, H. Masoud, H.A. Stone, Drag and diffusion coefficients of a spherical particle attached to a fluid-fluid interface, J. Fluid Mech. (2016). doi:10.1017/jfm.2016.41.

[72] J. Toro-Mendoza, G. Rodriguez-Lopez, O. Paredes-Altuve, Brownian diffusion of a particle at an air/liquid interface: The elastic (not viscous) response of the surface, Phys. Chem. Chem. Phys. 19 (2017) 9092–9095. doi:10.1039/c6cp07442a.

[73] G. Boniello, A. Stocco, C. Blanc, M. Nobili, Comment on “Brownian diffusion of a particle at an air/liquid interface: Elastic (not viscous) response of the surface,” Phys. Chem. Chem. Phys. 19

(2017) 22592–22593. doi:10.1039/c7cp02970e.

[74] J.C. Loudet, M. Qiu, J. Hemauer, J.J. Feng, Drag force on a particle straddling a fluid interface: Influence of interfacial deformations, Eur. Phys. J. E. 43 (2020). doi:10.1140/epje/i2020-11936-1.

[75] T. Ondarçuhu, A. Piednoir, Pinning of a contact line on nanometric steps during the dewetting of a terraced substrate, Nano Lett. 5 (2005) 1744–1750. doi:10.1021/nl051093r.

[76] D. Stamou, C. Duschl, D. Johannsmann, Long-range attraction between colloidal spheres at the air-water interface: the consequence of an irregular meniscus, Phys. Rev. E. Stat. Phys. Plasmas. Fluids. Relat. Interdiscip. Topics. 62 (2000) 5263–72.

[77] V. Carrasco-Fadanelli, R. Castillo, Measurement of the force between uncharged colloidal particles trapped at a flat air/water interface, Soft Matter. 15 (2019) 5815–5818. doi:10.1039/c9sm01051c.

[78] I.B. Liu, G. Bigazzi, N. Sharifi-Mood, L. Yao, K.J. Stebe, Curvature capillary repulsion, Phys. Rev. Fluids. 2 (2017). doi:10.1103/PhysRevFluids.2.100501.

[79] A. Wang, R. McGorty, D.M. Kaz, V.N. Manoharan, Contact-line pinning controls how quickly colloidal particles equilibrate with liquid interfaces, Soft Matter. 12 (2016) 8958–8967. doi:10.1039/c6sm01690a.

[80] S. Guo, M. Gao, X. Xiong, Y.J. Wang, X. Wang, P. Sheng, P. Tong, Direct measurement of friction of a fluctuating contact line, Phys. Rev. Lett. 111 (2013) 026101. doi:10.1103/PhysRevLett.111.026101.

[81] A. Giacomello, L. Schimmele, S. Dietrich, Wetting hysteresis induced by nanodefects, Proc. Natl. Acad. Sci. (2015) 201513942. doi:10.1073/pnas.1513942113.

[82] H. Perrin, D. Belardinelli, M. Sbragaglia, B. Andreotti, Response function of a moving contact line, Phys. Rev. Fluids. 3 (2018). doi:10.1103/PhysRevFluids.3.044001.

[83] E. Azar, C. Blanc, A. Mehdi, M. Nobili, A. Stocco, Mesoporous Silica Colloids: Wetting, Surface Diffusion and Cationic Surfactant Adsorption, J. Phys. Chem. C. 123 (2019) 26226–26235. doi:10.1021/acs.jpcc.9b05798.

[84] J. Meunier, D. Langevin, Optical reflectivity of a diffuse interface, J. Phys. 43 (1982) 185.

[85] T.M. Fischer, M. Sickert, F. Rondelez, Comment on “Shear viscosity of langmuir monolayers in the low-density limit”, Phys. Rev. Lett. 92 (2004) 139603–1.

[86] D. Langevin, Rheology of Adsorbed Surfactant Monolayers at Fluid Surfaces, Annu. Rev. Fluid Mech. 46 (2014) 47–65. doi:10.1146/annurev-fluid-010313-141403.

[87] N. Mucic, a Javadi, N.M. Kovalchuk, E. V Aksenenko, R. Miller, Dynamics of interfacial layers-experimental feasibilities of adsorption kinetics and dilational rheology., Adv. Colloid Interface Sci. 168 (2011) 167–78. doi:10.1016/j.cis.2011.06.001.

[88] F. Monroy, J. Giermanska Kahn, D. Langevin, Dilational viscoelasticity of surfactant monolayers, Colloids Surfaces A Physicochem. Eng. Asp. 143 (1998) 251–260. doi:10.1016/S0927-7757(98)00373-2.

[89] J. Giermanska-Kahn, F. Monroy, D. Langevin, Negative effective surface viscosities in insoluble fatty acid monolayers: effect of phase transitions on dilational viscoelasticity., Phys. Rev. E. Stat. Phys. Plasmas. Fluids. Relat. Interdiscip. Topics. 60 (1999) 7163–73.

[90] L. Liggieri, M. Ferrari, D. Mondelli, F. Ravera, Surface rheology as a tool for the investigation of processes internal to surfactant adsorption layers, Faraday Discuss. 129 (2005) 125. doi:10.1039/b405538a.

[91] F. Monroy, F. Ortega, R.G. Rubio, Dilatational rheology of insoluble polymer monolayers: Poly(vinylacetate), Phys. Rev. E - Stat. Physics, Plasmas, Fluids, Relat. Interdiscip. Top. 58 (1998) 7629–7641. doi:10.1103/PhysRevE.58.7629.

[92] A. Maestro, L.J. Bonales, H. Ritacco, T.M. Fischer, R.G. Rubio, F. Ortega, Surface rheology: macro- and microrheology of poly(tert-butyl acrylate) monolayers, Soft Matter. 7 (2011) 7761. doi:10.1039/c1sm05225j.

[93] P. Dhar, Y. Cao, T.M. Fischer, J.A. Zasadzinski, Active interfacial shear microrheology of aging protein films, Phys. Rev. Lett. 104 (2010) 1–4. doi:10.1103/PhysRevLett.104.016001.

[94] P. Dhar, T.M. Fischer, Y. Wang, T.E. Mallouk, W.F. Paxton, a Sen, Autonomously moving nanorods at a viscous interface., Nano Lett. 6 (2006) 66–72. doi:10.1021/nl052027s.

[95] L. Kramer, Theory of Light Scattering from Fluctuations of Membranes and Monolayers, J. Chem. Phys. 55 (1971) 2097–2105. doi:10.1063/1.1676380.

[96] D. Langevin, C. Griesmar, Light-scattering study of fatty acid monolayers, J. Phys. D. Appl. Phys. 13 (1980) 1189–1199. doi:10.1088/0022-3727/13/7/014.

[97] J.C. Earnshaw, P.J. Winch, Viscoelasticity of monolayers of n-pentadecanoic acid: A light scattering study, J. Phys. Condens. Matter. 2 (1990) 8499–8516. doi:10.1088/0953-8984/2/42/026.

[98] J. Agudo-Canalejo, R. Lipowsky, Critical particle sizes for the engulfment of nanoparticles by membranes and vesicles with bilayer asymmetry, ACS Nano. 9 (2015) 3704–3720. doi:10.1021/acsnano.5b01285.

[99] E. Evans, A. Yeung, Chemistry and Physics of LIPIDS Hidden dynamics in rapid changes of bilayer shape, Chem. Phys. Lipids. 73 (1994) 39–56.

[100] E. Evans, D. Needham, Physical properties of surfactant bilayer membranes: Thermal transitions, elasticity, rigidity, cohesion, and colloidal interactions, J. Phys. Chem. 91 (1987) 4219–4228. doi:10.1021/j100300a003.

[101] U. Seifert, Configurations of fluid membranes and vesicles, Adv. Phys. 46 (1997) 13–137.

doi:10.1080/00018739700101488.

[102] W.K. Den Otter, S.A. Shkulipa, Intermonolayer friction and surface shear viscosity of lipid bilayer membranes, Biophys. J. 93 (2007) 423–433. doi:10.1529/biophysj.107.105395.

[103] S.R. Tabaei, J.J.J. Gillissen, N.J. Cho, Probing Membrane Viscosity and Interleaflet Friction of Supported Lipid Bilayers by Tracking Electrostatically Adsorbed, Nano-Sized Vesicles, Small. 12 (2016) 6338–6344. doi:10.1002/smll.201601561.

[104] R. Lipowsky, The conformation of membranes., Nature. 349 (1991) 475. doi:10.1038/349475a0.